

# Supplementary Information

## **Calcium channel number critically influences synaptic strength and plasticity at the active zone**

Jiansong Sheng<sup>1</sup>, Liming He<sup>1</sup>, Hongwei Zheng<sup>2,3</sup>, Lei Xue<sup>1</sup>, Fujun Luo<sup>1</sup>, Wonchul Shin<sup>1</sup>, Tao Sun<sup>1</sup>, Thomas Kuner<sup>3</sup>, David Yue<sup>4</sup> and Ling-Gang Wu<sup>1</sup>

1. National Institute of Neurological Disorders and Stroke, 35 Convent Dr., Bldg 35, Rm. 2B-1012, Bethesda, Maryland 20892
2. Pharmacology Institute, Interdisciplinary Center for Scientific Computing, Heidelberg University, Heidelberg, Germany
3. Institute of Anatomy and Cell Biology, Heidelberg University, Heidelberg, Germany
4. Depts. of Biomedical Engineering and Neuroscience, Johns Hopkins University School of Medicine, Ross Bldg., Rm. 713, 720 Rutland Avenue, Baltimore, MD 21205

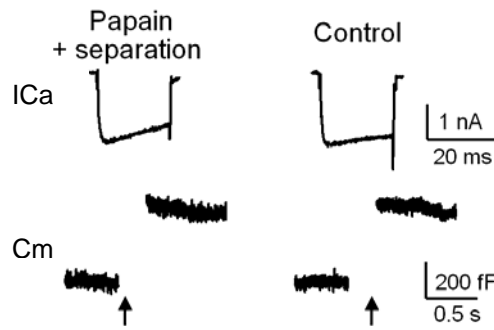


Figure S1. Sampled I<sub>Ca</sub> and C<sub>m</sub> induced by a 20 ms depolarization to 0 mV (arrow) at the calyx with (left) or without (right, control) papain treatment (2.5 unit/ml, bath application, 5 - 10 min) and exposure of the calyx release face calyx separation. Left and right panels are from different calyces.



Figure S2. No I<sub>Ca</sub> (lower) was induced by a 20 ms depolarization to 0 mV (upper) at a cell-attached patch at the release face of the calyx with 50  $\mu$ M cadmium in the pipette.



Figure S3. No I<sub>Ca</sub> was induced by a 20 ms depolarization to 0 mV from a cell-attached patch at the calyx outer face.

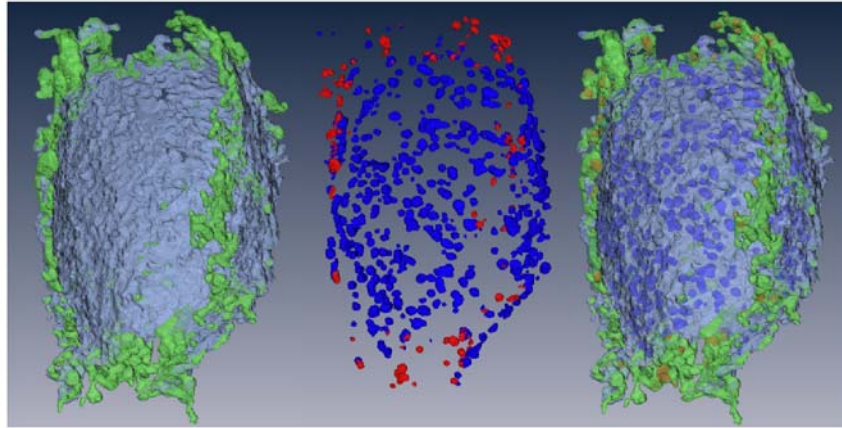


Figure S4, The active zone density is low at the rim region of a 3D reconstructed calyx. Confocal microscopic data were taken from Dondzillo, A. *et al. J Comp Neurol.* **518**, 1008-1029 (2010). Left: the GFP-labeled calyx rim (green) and center (light blue). Middle: the active zones (labeled with antibodies against bassoon and piccolo) in the rim (red) and center (dark blue) region. Right: Left and middle panels superimposed. The calyx vertical length is  $\sim 21 \mu\text{m}$ .

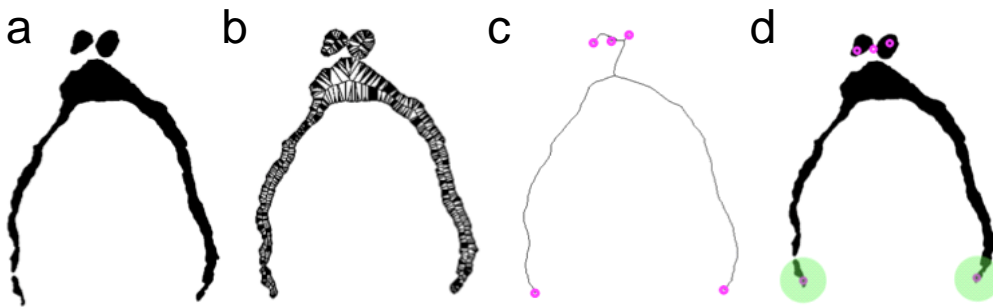


Figure S5. Workflow of detecting and segmenting rim and central parts of calyx sections. (a) Individual calyx section (binary representation). (b) Medial axis based skeleton. (c) Detection of ending points. (d) Label propagation to two right ending points are used as seed information for segmenting the rim parts from a calyx section.

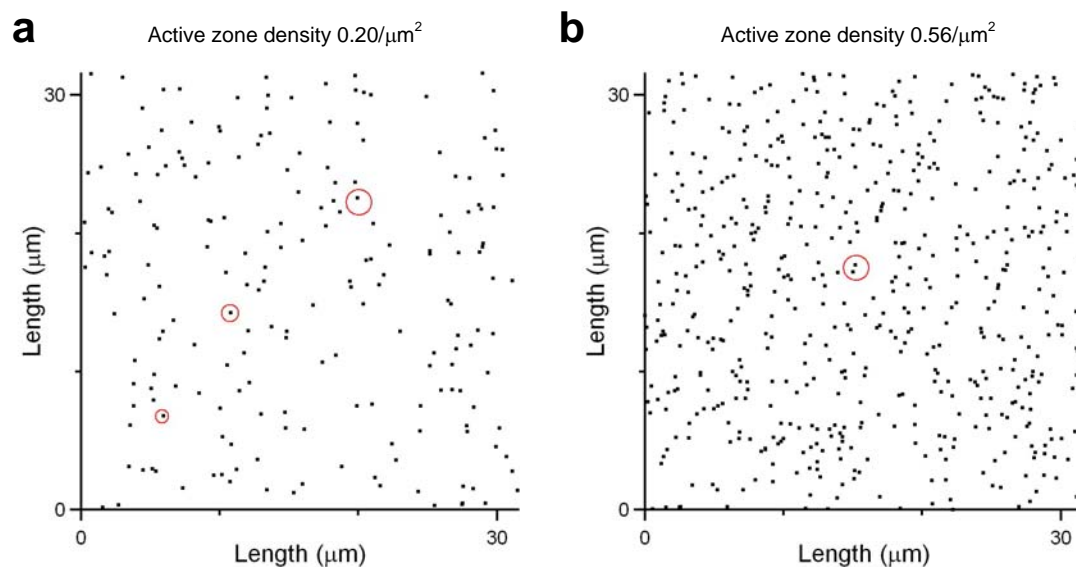


Figure S6. Parameters used for generating simulation results shown in Fig. 2b in the main text. (a) Active zones (dots) randomly distributed at a  $1000 \mu\text{m}^2$  square with an active zone density of  $0.2 \text{ active zone}/\mu\text{m}^2$ , the active zone density at the rim area measured from the electron microscopic data (Table S1). Three circles in the left show the mean membrane size of three different pipettes with resistance of  $12 - 14$ ,  $6 - 8$  and  $3 - 4 \text{ M}\Omega$ , respectively. These areas are  $0.67$ ,  $1.24$  and  $2.48 \mu\text{m}^2$ , respectively. The black bars shown in Fig. 2b (main text) were simulation results based on the settings shown here. (b) Active zones (dots) randomly distributed at a  $1000 \mu\text{m}^2$  square with an active zone density of  $0.56 \text{ active zone}/\mu\text{m}^2$ , the active zone density at the center area measured from the electron microscopic data (Table S1). The circle shows the mean membrane size of  $3 - 4 \text{ M}\Omega$  pipettes with an area of  $2.48 \mu\text{m}^2$ . The gray bars shown in Fig. 2b (main text) were simulation results based on the settings shown here.

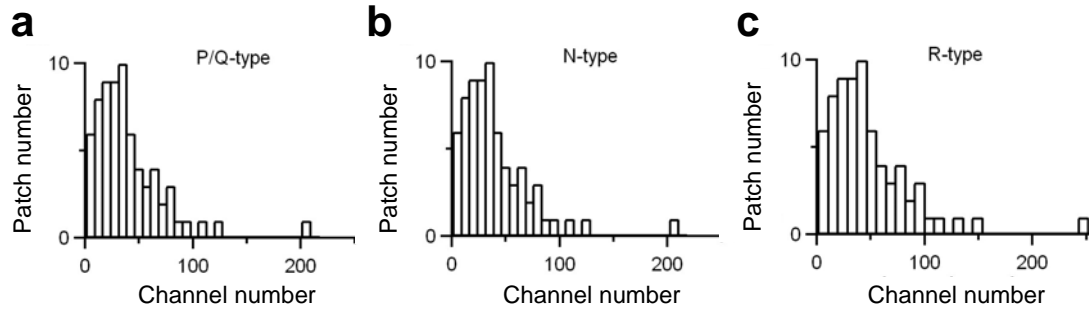


Figure S7. Distribution of the patch calcium number is similar regardless of the channel type used for calculation. The distribution of the patch calcium channel number derived from Fig. 1f, where the I<sub>Ca</sub> amplitude was converted to the calcium channel number using equation 1 in the main text. Panels a, b and c are similar except that  $i_{\text{mean\_channel}}$  and  $P_{\text{mean\_channel}}$  measured at  $V = 0$  mV are taken from P/Q-type alone, N-type alone and R-type alone, respectively. For P/Q-type,  $i_{\text{mean\_channel}}$  and  $P_{\text{mean\_channel}}$  at  $V = 0$  mV were  $0.27 \pm 0.01$  pA ( $n = 11$ ) and  $0.50 \pm 0.02$  (51 traces from 11 patches), respectively. For N-type,  $i_{\text{mean\_channel}}$  and  $P_{\text{mean\_channel}}$  at  $V = 0$  mV were  $0.28 \pm 0.01$  pA ( $n = 6$ ) and  $0.48 \pm 0.03$  (33 traces from 6 patches), respectively. For R-type,  $i_{\text{mean\_channel}}$  and  $P_{\text{mean\_channel}}$  at  $V = 0$  mV were  $0.26 \pm 0.01$  pA ( $n = 7$ ) and  $0.43 \pm 0.02$  (43 traces from 7 patches), respectively.

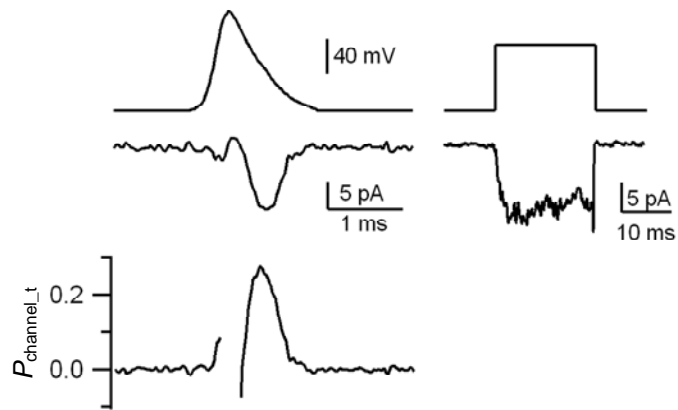


Figure S8. Low open probability of calcium channels during an action potential. Left: the I<sub>Ca</sub> (middle) and the VDCC open probability (lower, calculated from equation 2, main text) during an action potential waveform stimulus (upper). The experiment was similar to that shown in Fig. 7a (main text), except that the action potential waveform was scaled so that the half width was 0.16 ms wider (or 35% wider) as compared to that used in Fig. 7a in the main text. Right: I<sub>Ca</sub> (lower) induced by a 20 ms depolarization to 0 mV at 5 s after the action potential waveform stimulus (same patch as left).

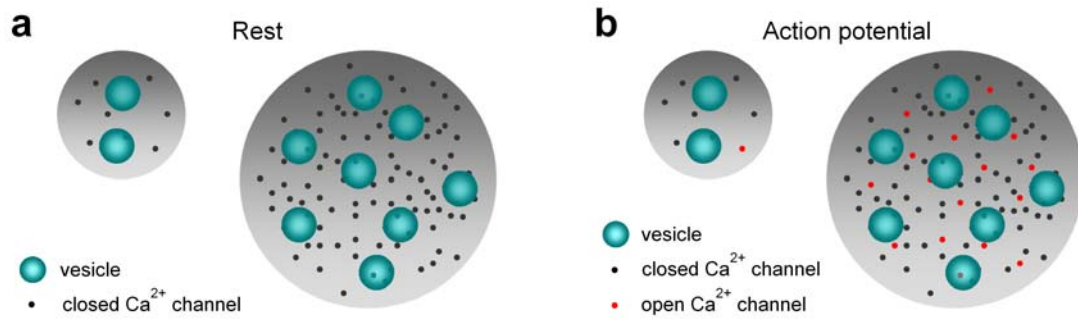


Figure S9. Graphic summary of the main finding. A Schematic drawing showing that as the calcium channel number increases at an active zone (left: active zone with few channels; right: active zone with many channels), the RRV number and the calcium channel number per RRV increases (a, resting condition), and the open calcium channel number during an action potential increases from ~1 to more than 10 (b, red, during an action potential). The drawing only serves for showing this finding visually. Other issues, like how channels are distributed at the active zone and the active zone size, should not be taken from this drawing.

	Surface density (active zone/ $\mu\text{m}^2$ )		
	Entire calyx	Center	Rim
Confocal microscopy	0.29 $\pm$ 0.01	0.32 $\pm$ 0.02	0.17 $\pm$ 0.02*
Electron microscopy	0.46	0.56	0.20

Table S1. Surface density of active zones. Data from confocal microscopy were expressed as mean  $\pm$  s.e.m. (n = 5 calyces, postnatal day 9). Data from electron microscopy were derived from a single reconstructed calyx (postnatal day 9). \*: significantly different from the density at the center region (p = 0.012, Mann Whitney test). Confocal microscopic data were from Dondzillo, A. *et al. J Comp Neurol.* **518**, 1008-1029 (2010). Electron microscopic data were from Sätzler, K. *et al. J Neurosci* **22**, 10567-10579 (2002).